Scripta Materialia 157 (2018) 120–123

Contents lists available at ScienceDirect

Scripta Materialia

journal homepage: www.elsevier.com/locate/scriptamat

Regular article

Impact of metastable phases on electrical properties of Si with different doping concentrations after processing by high-pressure torsion

Bumsoo Chon [a], Yoshifumi Ikoma [a,*], Masamichi Kohno [b,c], Junichiro Shiomi [d], Martha R. McCartney [e], David J. Smith [e], Zenji Horita [a,c]

[a] Department of Materials Science and Engineering, Faculty of Engineering, Kyushu University, Fukuoka 819-0395, Japan
[b] Department of Mechanical Engineering, Faculty of Engineering, Kyushu University, Fukuoka 819-0395, Japan
[c] International Institute of Carbon-Neutral Energy Research (I2CNER), Kyushu University, Fukuoka 819-0395, Japan
[d] Department of Mechanical Engineering, The University of Tokyo, Tokyo 113-8656, Japan
[e] Department of Physics, Arizona State University, Tempe, AZ 85287, USA

ARTICLE INFO

Article history:
Received 6 July 2018
Received in revised form 2 August 2018
Accepted 8 August 2018
Available online xxxx

Keywords:
Severe plastic deformation
High pressure torsion
Semiconductors
Electrical properties
Metastable phases

ABSTRACT

Si (100) wafers with various doping levels were subjected to high-pressure torsion (HPT). The resistivities for all doping levels increased by one or two orders of magnitude after initial compression, but then decreased after 10 revolutions of HPT processing to ~0.1 Ω cm for normally and heavily doped samples, and to ~0.02 Ω cm for the ultraheavily doped sample. After annealing at 873 K, the resistivities increased by four orders of magnitude compared to the original Si wafers. These results indicate that the formation of metastable phases plays an important role in the electrical resistivities of HPT-processed samples.

Crystalline Si transforms to various high pressure phases when high pressure is applied [1]. At ambient pressure and temperature, Si exhibits the diamond-cubic structure (Si-I) but it transforms to a tetragonal structure (Si-II) having metallic properties when the applied pressure is increased to ~9 GPa [2]. Further pressure increases lead to the formation of an orthorhombic structure (Si-XI) at ~13.5 GPa and a simple hexagonal structure (Si-V) at ~16 GPa [3]. When the pressure is reduced, reverse transformation occurs to Si-II, and then to a metastable body-centered-cubic structure (Si-III) and a rhombohedral structure (Si-XII) including Si-I [4]. The formation of Si-III and Si-XII are reported in high-pressure experiments [2–4] and indentation tests [5,6]. Since Si-III is a semimetal and Si-XII is a narrow band gap (0.24 eV) semiconductor [7], room-temperature writing of conductive zones involving Si-XII and Si-III phases has been demonstrated in Si by nanoindentation [5,6]. In addition, it has been reported that Si-III nanoparticles may be promising for multiple exciton generation based quantum solar cells, because of their lower optical band gap relative to Si-I nanoparticles [8].

Severe plastic deformation (SPD) through high-pressure torsion (HPT) [9,10] has been used for grain refinement of metallic materials [11] including allotropic phase transformations in Ti [12], Zr [13], and alloys such as Ti-Fe [14] and Co-Cu [15], and amorphization of crystalline phases in Nd–Fe–B alloy [16]. It has been observed that during HPT of metallic alloys the structure and properties of the samples quickly reach the steady state with increasing strain [17]. The HPT process has also been applied to semiconductors such as Si [18–22], Ge [23–26], and GaAs [27]. It was found that HPT-processed Si consisted of nanograins with Si-I, Si-III, and Si-XII crystal structures [19,20]. It was also observed that annealing of the HPT-processed samples at 873 K led to a nanograin structure with only Si-I [22], while a broad photoluminescence peak also appeared in association with the presence of the Si-I nanograins [19,20]. However, the effect of the dopant concentration on the Si microstructure and electrical conductivity has not so far been investigated. Thus, the objective of this study was to carry out HPT processing of Si wafers with different doping concentrations. We then measure electrical resistivities for samples after HPT processing and after successive annealing and also observe microstructure using high-resolution transmission electron microscopy (HRTEM).

We used Si (100) wafers with normal doping (10 Ω cm, *n*-Si), heavy doping (0.01 Ω cm, n^+-Si), and ultraheavy doping (0.0008 Ω cm, n^{++}-Si). The doping concentrations of the *n*, n^+, and n^{++}-Si wafers were estimated to be 5×10^{14}, 5×10^{18}, and 1×10^{21} atom/cm^3, respectively [28]. These wafers were cut into 5 mm diameter disks. HPT processing was conducted under a nominal pressure of 24 GPa with a rotation speed of 1 rpm at room temperature. The details of the HPT

* Corresponding author.
E-mail addresses: chon@zaiko6.zaiko.kyushu-u.ac.jp (B. Chon), ikoma@zaiko.kyushu-u.ac.jp (Y. Ikoma).

https://doi.org/10.1016/j.scriptamat.2018.08.011
1359-6462/

facility have been described elsewhere [13]. The HPT-processed samples were further annealed at 873 K in N_2 atmosphere for 1 h. Electrical resistivities of the HPT-processed samples before and after subsequent annealing, were measured by a four-point probe method (Mitsubishi Chemical Analytech Loresta-GP MCP-T610) with a probe distance of 1 mm. X-ray diffraction (XRD) profiles were obtained by a Rigaku SmartLab using Cu Kα radiation and micro-Raman spectra by HORIBA HR-800 using a laser wavelength of 488 nm. HRTEM observations were carried out using an image-corrected FEI Titan 80–300 operated at 300 kV. TEM specimens were prepared by crushing in isopropanol and then dispersing the powders onto holey carbon films.

Fig. 1 shows XRD profiles of the HPT-processed n-, n^+-, and n^{++}-Si samples after compression ($N = 0$), after 10 revolutions ($N = 10$), and following subsequent annealing. These XRD profiles show similar trends with respect to the HPT processing and the successive annealing regardless of the different dopant concentrations: only Si-I peaks are visible for $N = 0$, and additional Si-III and Si-XII peaks appear for $N = 10$, but no appreciable peaks such as metastable Si-IV are detected. The Si-III and Si-XII peaks disappear after annealing with only the Si-I peaks still remaining.

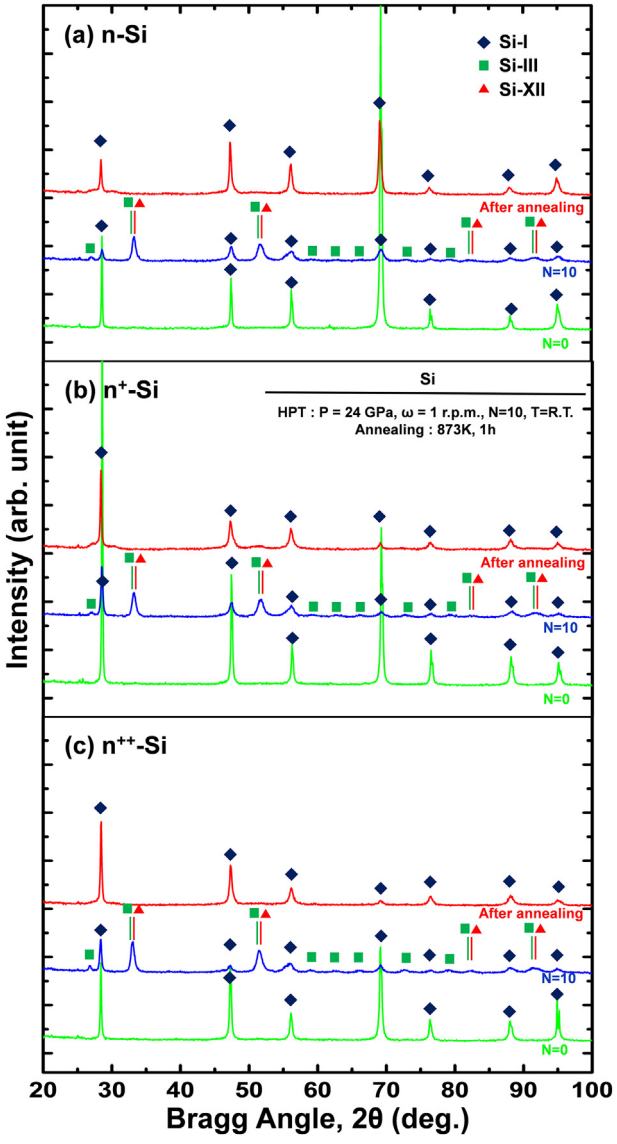

Fig. 1. XRD profiles of HPT-processed samples after compression ($N = 10$), for 10 revolutions ($N = 10$), and successive annealing after $N = 10$: (a) n-Si, (b) n^+-Si, and (c) n^{++}-Si.

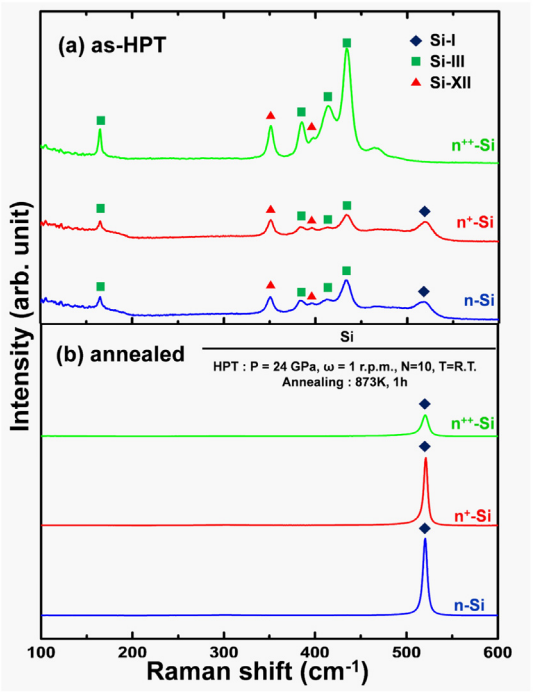

Fig. 2. Micro-Raman spectra of n-Si, n^+-Si, and n^{++}-Si, after (a) HPT processing for $N = 10$, and (b) annealing. Spectra were taken at 1.5 mm from disk center.

Fig. 2(a) and (b) shows Raman spectra of the HPT-processed n-, n^+-, and n^{++}-Si samples after processing through $N = 10$, and after successive annealing, respectively. In the HPT-processed samples, the presence of Si-III is confirmed by peaks around 160, 380, and 430 cm^{-1} [29] and Si-XII by the peak at 350 cm^{-1} [29], in addition to Si-I at 520 cm^{-1}, as shown in Fig. 2(a). It should be noted that the presence of Si-XII may be indistinguishable from the XRD profiles in Fig. 1 because the Si-XII peaks are close to the Si-III peaks. However, the Raman spectra clearly show the presence of Si-XII in all samples of doped Si after processing for $N = 10$. After annealing, these Si-III and Si-XII peaks disappear and only Si-I peaks at 520 cm^{-1} are observed, as shown in Fig. 2(b).

Fig. 3 shows an HRTEM image and corresponding fast Fourier transform (FFT) patterns for the HPT-processed n^{++}-Si sample with $N = 10$. Nanograins with sizes of several nm are marked by dotted lines, as well as amorphous regions, as shown in Fig. 3(a). The FFT patterns reveal the presence of Si-I having $[\bar{1}10]$ orientation and Si-III with $[0\bar{1}1]$ orientation,

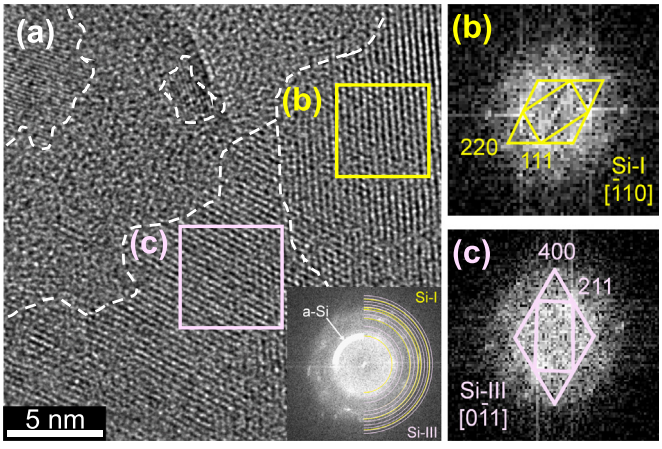

Fig. 3. (a) HRTEM image of HPT-processed n^{++}-Si for $N = 10$. (b, c) FFT patterns for square regions (b) and (c) in (a), respectively.